King's College London

MSc Project:

The random dimer covering problem on the weighted Aztec graph

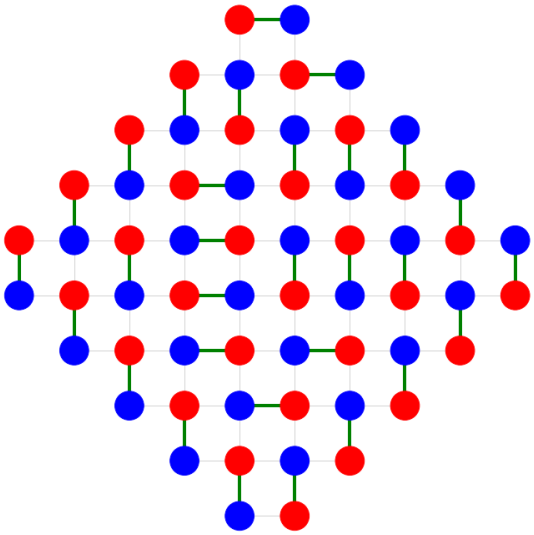

supervised by
Dr Gabriele Sicuro

23rd September, 2021

Acknowledgements

First of all, I would like to thank Dr Sicuro, for always having a positive mindset while always pushing me to improve and grow as a researcher.

Finally, thanks to my family and friends – you have always patiently listened and supported whatever I am up to in my studies, no matter how deep your understanding is or is not.

Contents

Abstract

Counting the number of possible tilings on a certain region is a problem that can be reformulated as the problem of counting perfect matchings on the pertinent dual graph. In this paper, we review some basic results, models and algorithms related to the dimer covering problem in order to study the random dimer problem on a very particular graph – the weighted Aztec graph. Not only we analysed the optimal solution at $T = 0$, but also explored the weighted Aztec graph at finite temperature regimes. Our intuition was that, in principle, the non-weighted Aztec diamond graph problem would be equivalent to the weighted one when averaging over many instances in the thermodynamic limit. However, it was shown that the arctic circle phenomenon does not arise for low temperatures in the weighted version.

1 Introduction

This manuscript is divided in two main parts:

1. The literature review, contained in Sections 2-4.
2. Methods and results, condensed in Section 5.

Generally, in the literature review, we introduce some basic concepts that will be needed to understand the problem at hand as well as earlier contributions to the analysis and solution to the dimer problem.

In Section 2, we define what a dimer covering and domino tiling is and discuss different methods to prove if a tiling is possible and state and outline the proof of the number of feasible dimer coverings in different regions. In this section we also introduce some definitions of graph theory that will be needed to define the random bipartite matching problem in the next section. Finally, we give a formal definition of the Aztec diamond region and graph, and state the most remarkable results on it.

In Section 3, we move onto combinatorial optimisation. We define the (monopartite) matching and bipartite matching problem, talk about their close relationship to statistical physics, and introduce the random bipartite matching problem. In this section we also briefly discuss some algorithms for assignment.

After introducing the main connections between combinatorics and statistical mechanics, in Section 4 we dive into describing some of the most important models of disordered systems in the context of physics. We discuss the main features of the Ising model and link these to glassy systems models. To finish this section, we state the main theory behind the cavity method and belief propagation, and describe how these can be applied to the assignment problem.

Finally, in Section 5 we define the weighted dimer problem on the Aztec graph, and present the main methods used to analyse the problem at hand, including loopy belief propagation. After discussing the results and outcomes of the project, we conclude our manuscript examining ways in which the project could be improved and future next steps.

2 Dimer coverings and domino tilings: some basic results

2.1 Introduction to dimer coverings and domino tilings

The dimer problem was firstly introduced to understand the thermodynamic properties of diatomic gas molecules (i.e., 'dimers') being absorbed onto a crystalline substrate [1]. Given a lattice with $2N$ sites, a **dimer covering** is an arrangement of N 'solid'

dimers such that every point of the lattice is covered by exactly one dimer. In Mathematics, this is usually called a **domino tiling**, with the dimers being the dominoes, and the domino tiling being a non-overlapping covering by such dominoes.

Starting with a region and a set of dominoes, we are interested in addressing questions like the existence of a tiling or how many tilings there are [2]. For example, can we tile with dominoes a 6×6 chessboard if we remove two squares from opposite corners? The key to answering this question hides in the apparently irrelevant characteristic black-and-white colouring of chessboards. In a domino tiling, each domino will lie exactly on one square of each colour. This implies that, for a domino tiling to exist, there must be the same number of black and white squares. Therefore, by removing two squares from opposite corners, which are the same colour, we conclude there is no tiling possible, as there are now 23 black squares and 21 white squares. This is an example of a **colouring argument** [2].

A fitting next step is to ask ourselves what happens when we remove one black square and one white square from the chessboard. This time we have the same number of black and white squares, which is a necessary condition, but it does not ensure that a tiling is possible. It is in fact possible to do so, and one can see that by considering any closed path that involves all the squares in the chessboard.

Although colouring arguments are widely used to prove the nonexistence of certain tilings, there are certain cases in which these are not enough. For instance, a triangular array of $\frac{n(n+1)}{2}$ unit regular hexagons, call it $T(n)$. For $n = 3$ or $n = 5$, this region cannot be covered with a tiling of *tribones*, regions formed by three close-packed hexagones, i.e., $T(2)$. John Conway discovered a way to show there does not exist a tiling for such regions by using combinatorial group theory techniques involving the Caley graph of a group (see [3]).

2.2 Tilings and graph theory: perfect matchings,

Another formulation of the tiling problem in combinatorial optimisation is that of **perfect matchings** in a bipartite graph, i.e., **the matching problem**. A domino tiling is equivalent to finding a perfect matching on a graph:

Definition 1: Perfect matching

Given an undirected graph $\mathcal{G} = (\mathcal{V}, \mathcal{E})$, a **matching** is a set of edges without common vertices. A **perfect matching** is a matching where every vertex is connected to exactly one edge, i.e., the matching involves all vertices in the graph.

The goal is to find a perfect matching such that a specific cost function is minimised. This idea will be formalised in the next section. The following theorem gives a criterion for the existence of a domino tiling on a graph.

Theorem 1: Hall's theorem

Given a bipartite graph $\mathcal{G} = (\mathcal{V}_1 \cup \mathcal{V}_2; \mathcal{E})$ there exists a perfect matching between the first vertex set $\mathcal{V}_1$ and the second vertex set $\mathcal{V}_2$ if and only if $\forall \mathcal{A} \subseteq \mathcal{V}_1$ we have $|\mathcal{A}| \leq |\mathcal{R}(A)|$ where $\mathcal{R}(\mathcal{A}) \subseteq \mathcal{V}_2$ is the set of adjacent vertices to $\mathcal{A}$.

In fact, **Hall's theorem helps us demonstrate that a tiling does not exist** [4, 2]. In order to show a tiling is impossible on a planar lattice, it is sufficient to find in the region $\mathcal{A}$ of k cells of one colour, say black, which have fewer than k neighbouring white cells.

2.3 Enumerating tilings

After having proved that a tiling problem can be solved, the focus is redirected to the number of possible tilings. One of the most important results about enumerating tilings is the number of domino tilings of a $m \times n$ chessboard $\mathcal{G}_{m,n}$.

Theorem 2: Tilings on a chessboard

The number of domino tilings of a $m \times n$ chessboard (m and n even) is

$$\prod_{j=1}^{\frac{m}{2}} \prod_{k=1}^{\frac{n}{2}} \left(4\cos^2 \frac{j\pi}{m+1} + 4\cos^2 \frac{k\pi}{n+1} \right). \tag{1}$$

This theorem was obtained independently in 1961 by Kasteleyn [5] and by Fisher and Temperley [6]. It is an outstanding formula since the numbers that are being multiplied are often not even rational number, but still the formula gives an integer as a result of this multiplication. In the following paragraphs, we will briefly review the main methods used to prove Theorem 1 in both papers.

In [5], Kasteleyn stated that the number of tilings of a $m \times n$ chessboard or the number of perfect matchings of the corresponding bipartite planar graph $\mathcal{G}_{n,m}$ is given by the pfaffian of the Kasteleyn matrix. In order to state Kasteleyn's theorem, we need a few other definitions first.

Definition 2: Kasteleyn weight

Given two vertices in $\mathcal{G}_{n,m}$, u and v, we define the *Kasteleyn weight* $w(u, v)$ as:

$$w(u,v) = \begin{cases} 1 & \text{if } (u,v) \text{ is a horizontal edge} \\ i & \text{if } (u,v) \text{ is a vertical edge} \\ 0 & \text{else} \end{cases}$$

A Kasteleyn-weighted grid graph $\mathcal{G}'_{n,m}$ is the grid graph $\mathcal{G}_{n,m}$ where the edges are weighted according to the Kasteleyn weight.

We may now state Kasteleyn's Theorem.

Theorem 3: Kasteleyn's theorem

Define the Kasteleyn matrix $K_{n,m}$ to be the adjacency matrix of the Kasteleyn-weighted grid graph $\mathcal{G}'_{n,m}$. Then, the number of perfect matchings of $\mathcal{G}_{n,m}$ is given by $\sqrt{|\det(K_{n,m})|}$.

By calculating the eigenvalues of $K_{n,m}$, Kasteleyn obtained the announced formula for the $m \times n$ chessboard:

$$T_{n,m} = \Big| \prod_{j=1}^{m} \prod_{k=1}^{n} \left(2\cos\frac{j\pi}{m+1} + 2i\cos\frac{k\pi}{n+1} \right) \Big|^{\frac{1}{2}} \tag{2}$$

Remark 1:

For n, m even, one can arrive to Eq. 1 from Eq. (2):

$$\begin{aligned} T_{n,m} &= \Big| \prod_{j=1}^{m} \prod_{k=1}^{n} \left(2\cos\frac{j\pi}{m+1} + 2i\cos\frac{k\pi}{n+1} \right) \Big|^{\frac{1}{2}} = \\ &= \prod_{j=1}^{m} \prod_{k=1}^{n} \left(4\cos^2\frac{j\pi}{m+1} + 4\cos^2\frac{k\pi}{n+1} \right)^{\frac{1}{4}} = \\ &= \prod_{j=1}^{m} \prod_{k=1}^{n} \left(4\cos^2\frac{j\pi}{m+1} + 4\cos^2\frac{k\pi}{n+1} \right)^{\frac{1}{4}} = \\ &= \prod_{j=1}^{\frac{m}{2}} \prod_{k=1}^{\frac{n}{2}} \left(4\cos^2\frac{j\pi}{m+1} + 4\cos^2\frac{k\pi}{n+1} \right) \end{aligned}$$

Fisher and Temperley [6] got to the same result as Kasteleyn by obtaining a partition function (statistical mechanical object that will be defined further on), and with some operator techniques, they reduced it to a Pfaffian [7]. Later on, in 1967, Elliot Lieb published a very elegant proof which used a technique that is widely used in enumerative combinatorics and statistical mechanics – the transfer matrix method [8].

In both papers, Kasteleyn's and Temperley and Fisher's, they showed the following result for $2n \times 2n$ square chessboards [2]:

Theorem 4: Asymptotic number of domino tilings

The number of domino tilings of a $2n \times 2n$ square is approximately C^{4n^2} with $C = e^{\frac{G}{\pi}} = 1.338515152\ldots$. G is the Catalan constant, which is defined by

$$G = \sum_{n=0}^{\infty} \frac{(-1)^n}{(2n+1)^2} = 0.915965594\ldots$$

2.4 The Aztec diamond

The main focus of this project is studying the statistics of the tilings of the Aztec diamond. The **Aztec diamond** of order n is a region constituted by all unit squares of a square lattice whose centers (x, y) fulfill $|x| + |y| \leq n$, where n is a fixed integer. Notice that x and y are half-integers. For example, for $n = 3$

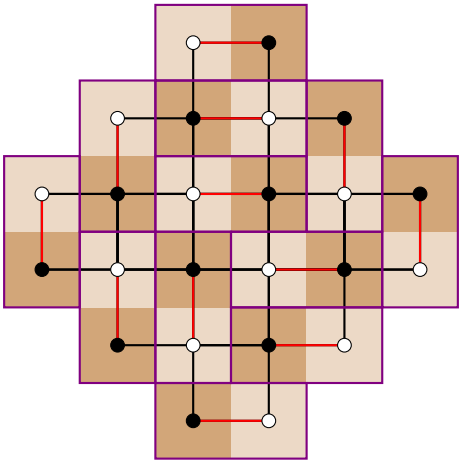

The **Aztec diamond *graph*** of order n is the dual graph of the Aztec diamond (defined above) where the vertices correspond to the squares and the edges between two vertices exist if and only if the equivalent squares in the aztec diamond are adjacent [9]. Identifying each 'chosen' edge in a perfect matching with a domino of the tiling in the Aztec diamond, it is not difficult to intuit that there is a bijection between the perfect matchings on the Aztec diamond graph and the domino tilings of the Aztec diamond [9], as it was described for any type of graph generally in the previous section.

As we increase n, one can see that the Aztec tilings are constituted by a circular region where the tiles exhibit well-mixed orientations, and four regions surrounding it with a "brick-wall" pattern [10] (see Figure 1). These two well-differentiated regions are usually called the **temperate zone** and the **frozen region** respectively. Their appearance constitute **the arctic circle phenomenon**, and it is described by the following theorem.

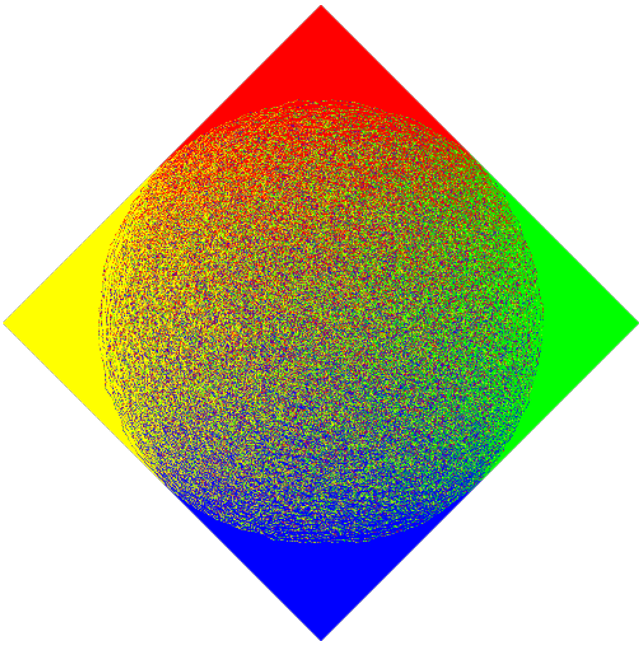

Figure 1: Example of Aztec Diamond of order $n = 1000$ drawn uniformly where the arctic circle phenomenom can be observed. The tiles in the corner correspond to the frozen regions, and the tiles with mixed orientations in the circle, to the temperate zone. In this picture adapted from online resources of Université catholique de Louvain (see https://sites.uclouvain.be/aztecdiamond/), north, south, west and east dominoes are painted respectively in red, blue, yellow and green. The algorithm used to produce this Aztec Diamond is a modified version of Propp's Generalised Domino Shuffling algorithm [11, 12].

Theorem 5: The Arctic Circle theorem

Let $\epsilon > 0$. Then, for all sufficiently large n, all but an ϵ fraction of the domino tilings of the Aztec diamond of order n will have a temperate zone whose boundary stays uniformly within distance ϵn of the inscribed circle.

Another crucial result proved by Elkies, Kuperberg, Larsen and Propp in [13] is the number of tilings of the Aztec diamond:

Theorem 6: Tilings on the Aztec diamond

The number of domino tilings of the Aztec diamond of order n is $2^{\frac{n(n+1)}{2}}$.

Remark 2:

The Aztec diamond has $T = 2^{\frac{n(n+1)}{2}}$ tilings and consists of $N = 2n(n+1)$ squares. This means that the number of degrees of freedom per square is $\sqrt[N]{T} = 1.189207115\ldots$ [2]. For the $2n \times 2n$ chessboard, the degrees of freedom per square is approximately $C = 1.338515152\ldots$ from Theorem 3. This means that the intuition that it is 'simpler' to tile a square board than the Aztec diamond is indeed correct.

In [13], there are four different proofs given for Theorem 5, including the celebrated **domino shuffling algorithm** [11]. Here, we will explore the first proof given. A bijection is established between tilings of the Aztec diamonds and height functions, and the lattice structure of alternating sign matrices is exploited.

Definition 3: Height function

The height function H_T is defined as follows:

1. Start at a reference vertex v_0 of some domino where the height will be 0.
2. Take an edge-path γ from v_0 to some other vertex v.
3. Along γ, the height can vary ± 1 along each edge.
4. Given a standard black-and-white coloring of the chessboard, if there is a black square on the left of the edge being traversed, the height increases by 1. Otherwise, it decreases by 1.

H_T satisfies the following properties [14]:

- H_T takes the subsequent values when moving counterclockwise along the boundary of the Aztec diamond: $0, 1, \ldots, 2n+1, 2n+2, 2n+1, \ldots, 0, \ldots, 2n+1, 2n+2, 2n+1, \ldots, 0$.

- When moving from one vertex v_1 to another v_2 we have that either $H_T(v_2) = H_T(v_1) + 1$ or $H_T(v_2) = H_T(v_1) - 3$.

Every function that satisfies these two conditions defines a domino tiling.

The height function is a $\mathbb{Z}$-valued function defined on the vertices of the tiling, and up to an additive constant and can be thought of as a way of extending a 2-dimensional domino tiling to 3D.
Given a height function like the one shown in Figure 2 (left), by rotating it 45º, one obtains two matrices defined by the even and odd rows of the right image in Figure 2 respectively. These, up to re-scaling, represent the extended matrices of two alternating-sign matrices.

Definition 4: Alternating-sign matrices and their extended matrices

Alternating-sign matrices are a special type of combinatorial matrices. They are square matrices with entries of 0, 1 and -1 such that the nonzero elements in each row and column alternate sign and the sum of each row and column is 1.
Let $A = (a_{i,j})_{i\leq i,j\leq n}$ be an alternating-sign matrix of order n. Then, we define its **extended matrix** $A^* = (a^*_{r,s})_{i\leq r,s\leq n}$ of order $n+1$ as

$$a^*_{r,s} = r + s - 2\sum_{i=1}^{r}\sum_{j=1}^{s} a_{i,j}.$$

There is a **bijection** between alternating-sign matrices of order n and their extended matrices.

One can reconstruct the domino tiling of the Aztec diamond from this special pair of matrices. And, by looking at how the two alternating-sign matrices are related, a recurrence relation over the number of tilings of Aztec diamonds of order n and $n-1$ [13] can be obtained. The proof of Theorem 5 relies on these properties of alternating-sign matrices constructed on the Aztec diamond.

Remark 3: The number of alternating-sign matrices and Statistical Physics

The **number of alternating-sign matrices of order** n was conjectured to be

$$\prod_{j=0}^{n-1} \frac{(3j+1)!}{(n+j)!}$$

by Mills, Robbins, and Rumsey in [15]. Later on, this formula was proved by Zeilberger [16] and by Kuperberger [17] in 1996. Kuperberg's proof was more

concise than Zeilberger's and showed there is a one-to-one correspondence between alternating-sign matrices and a configuration from statistical physics called the **six-vertex model or square ice model**. This illustrates one of the many connections between combinatorics, domino tilings, and statistical physics (see section 5).

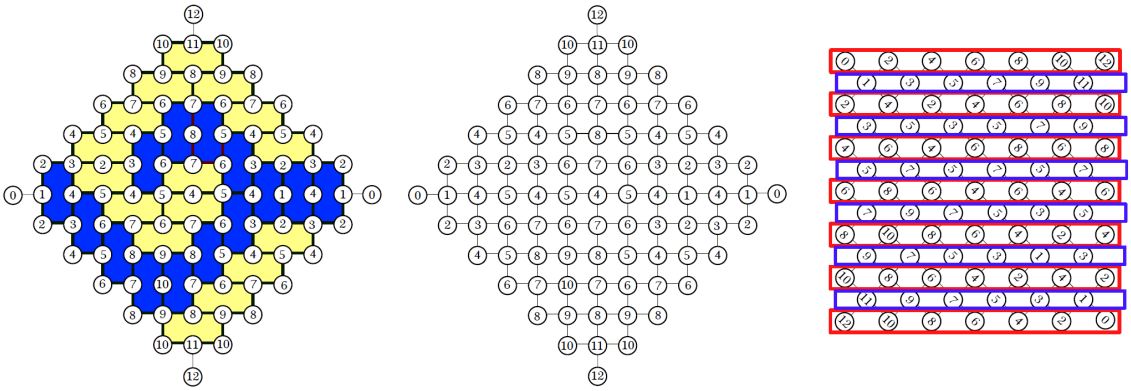

Figure 2: Example of Aztec Diamond tiling (left) and its height function (centre) (adapted from [14]). The image on the right originates from the rotation of the Aztec diamond clockwise by $\frac{\pi}{4}$. The even rows highlighted in blue define the matrix A, and the odd ones in red, B. Upon correct normalisation, they represent the extended matrices of two alternating-sign matrices. From this unique pair and their relation between each other, one can reconstruct the domino tilings and prove Theorem 5.

Another feature of the height functions that is closely related to statistical mechanics is conformal invariance.

Theorem 7: Conformal invariance of the height function on domino tilings

The scaling limit of the height function, i.e. when the lattice spacing approaches zero, tends to the **massless Gaussian free field** [18]. This is a conformally invariant continuous process that is a natural d-dimensional-time analog of Brownian motion [19].

3 The random bipartite matching problem

3.1 The matching problem and the bipartite matching problem (BMP)

In the previous section, we discussed the number of possible configurations of dominoes on a chessboard and on the Aztec diamond. To do so, we aided ourselves with graph theory and combinatorics. We also commented on some of the connections to statistical physics. The reality is that the relationship between domino tilings and statistical physics is much deeper than we have described up to this point. We will motivate this point in the following paragraphs.

Now, imagine we associate a weight to each pair of squares where we can place a domino. This is equivalent to having weights associated to each edge on the region's corresponding dual graph, i.e.,

Definition 5: Weighted graph

Define a function $w : \mathcal{E} \to \mathbb{R}$, which we associate to the graph $\mathcal{G} = (\mathcal{V}, \mathcal{E})$. Given an edge $e \in \mathcal{E}$, we call $w(e)$ the **weight** of e.

When we consider a weighted graph, our main goal switches from counting configurations or *feasible solutions* to finding the *optimal solution* amongst all possible solutions. This is a combinatorial optimisation problem, where the number of feasible solutions, i.e., the number of possible tilings, can be extremely large, but is nonetheless finite.

In order to formalise this idea, let us define the **k-assignment problem**.

Definition 6: The k-assignment problem

Consider the **complete** weighted **bipartite** graph $\mathcal{K}_{N,M} = (\mathcal{V}_1 \cup \mathcal{V}_2,\ \mathcal{E})$ with weight function $w : \mathcal{E} \to \mathbb{R}^+$, and cardinality $k \leq \min\{N, M\}$. In the k-assignment problem, we aim to find a perfect matching $M \subseteq \mathcal{K}_{N,M}$ with $\mathcal{E}_M \subseteq \mathcal{E}$ such that the cost functional

$$\mathcal{C}[M] \coloneqq \frac{1}{|\mathcal{E}_M|} \sum_{e \in \mathcal{E}_M} w(e) \tag{3}$$

is minimised.

Remark 4: The cardinality matching problem

When $w(e) = 1\ \forall e$, the goal is to find a matching with as many edges as possible as long as each vertex is adjacent to at most one edge. This is sometimes referred to as the **cardinality matching problem**. Finding a possible domino tiling in

a region is analogous to finding a cardinality matching on its dual graph. This is the case we have been studying so far, where all we were doing was counting configurations, rather than finding the one(s) that optimises the cost.

Particularly, when the k-assignment problem is formulated on the complete bipartite graph $\mathcal{K}_{N,N}$, i.e. the N-assignment problem, we call it the **bipartite matching problem** or the **assignment problem (BMP)** [20]. One of the most celebrated algorithms for the solution of the assignment problem is the *Hungarian algorithm* [21], an algorithm with polynomial computational complexity.

Remark 5: The generalised bipartite matching problem

The BMP can be defined on an arbitrary bipartite non-directed graph $\mathcal{G} = (\mathcal{V}_1 \cup \mathcal{V}_2,\ \mathcal{E})$, as long as $|V_1| = |V_2|$. This allows us to study the weighted dimer covering problem on different regions, such as the Aztec diamond. For simplicity, we will refer to this generalisation from now on as the BMP.

Remark 6: Other algorithms for assignment

Apart from the Hungarian algorithm which was designed to solve the assignment problem, there are other algorithms that can be used. For example, the **simplex method** [22]. It is originally intended for linear optimisation problems, but since the assignment problem can be reformulated as a linear optimisation problem [20], the simplex method can be used to solve it. Another two remarkable algorithms are **belief propagation** [23], which is based on the cavity method, and the **domino shuffling algorithm**. The latter was devised specifically to get the sum of the weights associated to the matchings of the weighted Aztec diamond graph.

3.2 From combinatorics to statistical physics

There is a direct relationship between optimisation problems and statistical physics [23]. Given the bipartite matching problem, one can explore its natural mapping to statistical mechanics by introducing the **Boltzmann distribution**.

Let χ be the space of configurations. This set contains all possible matchings M or dimer coverings of a particular graph. Let the cost or energy function be $C(M)$, defined as in Eq. 3. For any $\beta = \frac{1}{T}$ with $T \equiv$ temperature, each matching M is assigned a probability

$$p_\beta(M) = \frac{e^{-\beta C(M)}}{Z(\beta)} \tag{4}$$

with

$$Z(\beta) = \sum_{M \in \chi} e^{-\beta C(M)}, \tag{5}$$

where $p_\beta(M)$ is the Boltzmann distribution and $Z(\beta)$ is the partition function of the system, a normalisation constant. Notice that both T and therefore, β are positive parameters.

When $\beta \to \infty$, the exponentials that dominate are the ones with the lowest energies, i.e., the probability concentrates on the ground states. Hence, in this limit we recover the optimisation problem, where we want to look at optimal or minimum costs.

In the limit of infinite T, as $\beta \to 0$, $p_\beta(M) = 1 \; \forall M$. This means that all matchings are equally likely. In a way, it is as if the weights of the edges were set to be the same and therefore, we are back at counting all possible matchings, regardless of their cost.

In statistical mechanics, when a system is at thermal equilibrium with a heat bath at fixed T, the probability that the system will be in a certain state is given by the Boltzmann distribution. In many cases, a thorough analysis of the properties of the system at finite β can give key insights about the behaviour of the system.

Some of the most important quantities are the thermodynamical potentials, as they represent the thermodynamic state of the system. In particular, the **Helmholtz free energy**. It is the work available for use to a system at constant T and volume.

Definition 7: The thermodynamic potentials

The **Helmholtz free energy** can be expressed in terms of the partition function as follows

$$F(\beta) = -\frac{1}{\beta} \ln Z(\beta)$$

or in term of the **canonical entropy** $S(\beta)$ and the **internal energy** as

$$F(\beta) = U(\beta) - \frac{1}{\beta} S(\beta) \ ,$$

where

$$U(\beta) = \langle C(M) \rangle = \sum_{M \in \chi} p_\beta(M) \, C(M) \ ;$$
$$S(\beta) = -\sum_{M \in \chi} p_\beta(M) \ln p_\beta(M).$$

Remark 7:

Notice that all the thermodynamic potentials above were defined with respect to the bipartite matching problem where the energy of the system is the cost of the matching, and the weights of the edges are the cost that the system pays when an edge is amongst the edges of a matching.

Remark 8: The partition function as a product of partition functions

We have that

$$Z(\beta) = \sum_{M\in\chi} e^{-\beta C(M)} = \sum_{M\in\chi} e^{-\beta\sum_{e\in\mathcal{E}_M}\frac{w(e)}{|\mathcal{E}_M|}} =$$
$$= \sum_{M\in\chi}\prod_{e\in\mathcal{E}_M} e^{-\beta\frac{w(e)}{|\mathcal{E}_M|}} = \prod_{e\in\mathcal{E}_M}\sum_{M\in\chi} e^{-\beta\frac{w(e)}{|\mathcal{E}_M|}} = \prod_{e\in\mathcal{E}_M} Z_e(\beta)$$

where $Z_e(\beta) = \sum_{M\in\chi} e^{-\beta\frac{w(e)}{|\mathcal{E}_M|}}$ is the partition function of the sub-system of the edges of the perfect matchings.

Remark 9: The thermodynamic limit

Since the number of particles N of thermodynamical systems is typically of order 10^{23}, statistical physicists normally focus on the $N \to \infty$ limit, also called the **thermodynamic limit** [23]. In this limit, thermodynamic potentials are $\mathcal{O}(N)$, and the system becomes translationally invariant [24]. Therefore, it is convenient to introduce the **intensive thermodynamic potentials**, which do not depend on the quantity of 'substance' that we are looking at. To do so, we just divide by N our 'original' potentials and take the limit, assuming it exists. In the case of the bipartite matching problem, we will divide through the number of nodes of the graph in order to ensure this well-behaviour on the limit of large graphs.

3.3 The random bipartite matching problem (RBMP) and statistical mechanics

In the bipartite matching problem, we assumed that, once the optimisation problem was defined, the parameters of the graph (e.g. the weights) were fixed and the same for all instances. In reality, this need not be the case.

In order to examine in more depth the *typical* features of a given optimisation problem, it is convenient to collect data from many instances and study its solution on average, and for very large inputs. The statistical nature of this approach lead statistical physics to play a crucial role in developing new techniques for this type of problems.

Definition 8: The random bipartite matching problem

In the random bipartite matching problem (RBMP) or random assignment problem on the complete graph $\mathcal{K}_{N,M} = (\mathcal{V}_1 \cup \mathcal{V}_2,\ \mathcal{E})$, the weights $\{w(e)\}_{e\in\mathcal{E}}$ are **random variables** drawn from a specific probability distribution.

Remark 10:

In the simplest scenario, the weights are **independently and identically distributed (i.i.d.) random variables**, i.e., they all have the same probability distribution, say $\rho(w)$, but are mutually independent.

Remark 11:

The weights being drawn from a probability distribution independently defines on itself a collection of random instances of the problem. We are interested in properties like the average optimal cost or the optimal cost distribution for a given number of realisations in the thermodynamic limit [20].

In [25], Aldous studied rigorously the RBMP in the thermodynamical limit for i.i.d weights with probability distribution $\rho(w) = \theta(w)\ e^{-w}$, proving the formulas obtained by Mézard and Parisi in 1985. By constructing Poisson-weighted infinite trees (i.e. unfolding maps) from the weighted complete graph, being deeply inspired by the cavity method (firstly designed for glassy systems), Aldous proved the following results:

Theorem 8:

The distribution of the weights on the edges of the optimal matching is

$$\rho_0(w) = \theta(w)\frac{e^{-w} + w - 1}{4\sinh^2\frac{w}{2}}. \tag{6}$$

Corollary 1: AOC of the RBMP

The **average** optimal cost (AOC) of the RBMP in the thermodynamical limit is

$$\lim_{N\to\infty} \mathcal{C}_N^{RBMP} = \int_0^\infty w\rho_0(w)\mathrm{d}w = \frac{\pi^2}{6} \tag{7}$$

Remark 12:

Mezard and Parisi already got Eq. 6 and Eq. 7 in 1985 using the replica approach [26], which we will outline in the next section.

However, Eq. 7 does not provide any information about finite size corrections. Parisi conjectured in 1998 [27] a formula for the average cost of the assignment problem on the complete graph with exponential weight distribution for finite N.

Theorem 9:

In the **random assignment problem**, the average optimal cost is

$$\mathcal{C}_N^{RBMP} = \sum_{i=1}^{N} \frac{1}{i^2} \tag{8}$$

Remark 13:

The RBMP can be formulated on a generic graph $\mathcal{G}$, just like the BMP. In section 5, we will focus our analysis on the statistics of the weighted dimer covering problem (or RBMP) on the Aztec diamond graph.

4 Disordered systems and random assignment

The fact that Statistical physics deals with large systems involving many degrees of freedom subject to constraints and interactions, led physicists to develop general tools for the investigation of this kind of problems. As an example, let us start introducing a simple model, the Ising model. We will discuss then an algorithm used to solve this (and many similar models) on graphs and finally its application to matching problems.

4.1 Ising model

One of the simplest models of interacting many-body systems is the *Ising model*. It was firstly introduced to understand *phase transitions* in magnetic systems [28] by looking at the interaction of the system's binary units.

Let us consider a generic graph $\mathcal{G}$. The graph can be, for example, a cubic lattice $\mathcal{C} = \{1, 2, \dots, L\}^d \equiv \{i\}_{i=1,\dots,N}$ in d dimensions with side length L and $N = L^d$ points, where each element or point i is a *site*. In Figure 3 the 2-d lattice is a grid graph of 6 by 6, and the nodes, represented by the blue points, are the sites.

A site could be anything from a lattice point on a crystal to a neuron in a neural network [29], but for now, we will adhere to the terminology used in ferromagnetism for simplicity.

Each of the sites is assigned a variable σ_i called the *spin*. It is characterised by the binary value $\sigma_i = \pm 1$. In ferromagnetism, the *Ising spin* represents the microscopic magnetic moment [29]. If the spin is pointing up ($\uparrow$), $\sigma_i = +1$, and if it is pointing down

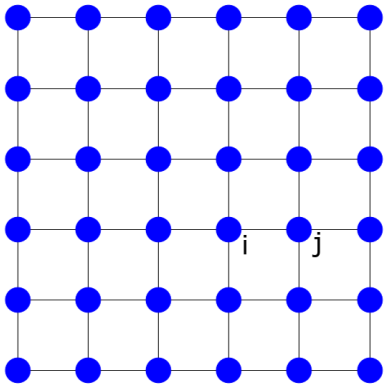

Figure 3: Example of 2-dimensional lattice of side $L = 6$. The blue points represent the sites, and (ij) is a bond of neighbouring sites.

$(\downarrow)$, $\sigma_i = -1$. In the model, sites interact with their nearest neighbours. In a lattice of dimension d, each site has $2d$ nearest neighbours. A pair of connected sites (ij) is called a *bond*. To each bond, we assign an *interaction energy* $-J\sigma_i\sigma_j$. Thus, the interaction energy of (ij) is

$$E_{(ij)} = \begin{cases} -J & \text{if } \sigma_i = \sigma_j \\ +J & \text{otherwise} \end{cases}$$

The size of J modulates the strength of the interaction or coupling of the spins, whereas the sign of J denotes if it is energetically more favourable for neighbouring spins to align ($\uparrow\uparrow$ or $\downarrow\downarrow$) or anti-align ($\uparrow\downarrow$).

In the case of $J > 0$, the state where the two spins are the same has a lower energy, meaning that it is more stable, and that all pairs of spins will tend to have the same orientation [29]. This leads to macroscopic magnetism, and the interaction is said to be *ferromagnetic*. On the other hand, when $J < 0$, antiparallel arrangements are favoured. In this case the interaction is said to be *antiferromagnetic*. A configuration $\vec{\sigma} = (\sigma_1, \ldots, \sigma_N)$, with $\sigma_i \in \{-1, +1\}$ being the spin of the ith site, has energy function or Hamiltonian

$$E(\vec{\sigma}) = -J \sum_{(ij)} \sigma_i \sigma_j - h \sum_{i \in \mathcal{C}} \sigma_i, \tag{9}$$

where the first sum runs over all the couples of sites i, j that are nearest neighbours. The second term in the energy function corresponds to the *Zeeman energy*, and $h \in \mathbb{R}$ measures the applied external magnetic field [23]. Assuming now that the system is in contact with a thermal bath at temperature $T = \beta^{-1}$, a goal of statistical physics is to estimate the statistical properties of the system given that the configuration $\vec{\sigma}$ is visited

in the evolution of the system with probability

$$P(\vec{\sigma}) = \frac{1}{Z(\beta)} e^{-\beta E(\vec{\sigma})}, \qquad Z(\beta) = \sum_{\vec{\sigma}} e^{-\beta E(\vec{\sigma})}. \tag{10}$$

Remark 14:

Calculating the free energy density $f(\beta)$ in the thermodynamic limit is not an easy task. So far, Ising solved the $d = 1$ in 1924 and showed there are not phase transitions. In 1948, Onsager solved it for the 2-dimensional case, where there is a second order phase transition. The problem remains unsolved for higher dimensions, but the main features of the solution are known.

Let us discuss qualitatively what we can expect from the properties of this model. In the limit of infinite temperature, all configurations 'weigh' the same in the Boltzmann distribution, so the spins are completely independent. As $T \to 0$, the Boltzmann distribution concentrates on the ground states. When there is no external magnetic field, there are two degenerate ground states: one where all spins point up, and other one where they all point down. When we turn back on the magnetic field, one of the two configurations prevails: $\vec{\sigma}^{(+)} = (+1, \ldots, +1)$ for $h > 0$ and $\vec{\sigma}^{(-)} = (-1, \ldots, -1)$ for $h < 0$.

Remark 15:

In dimensions higher or equal than $d = 2$, the spontaneous magnetisation, a quantity that represents a cooperative response to the magnetic field, can be non-zero for $\beta > \beta_c$. This is the so called **ferromagnetic phase**. For $\beta < \beta_c$, the spontaneous magnetisation is 0, and we are in a **paramagnetic phase**. There is a phase transition at $\beta = \beta_c$. Note that for the case $d = 1$, $\beta_c = \infty$ and there is no phase transition.

4.2 Spin glasses and solution by replicas

Let us consider now an Ising-type model on a generic graph $\mathcal{G}$ with energy function

$$E(\vec{\sigma}) = -\sum_{(ij)} J_{ij}\sigma_i\sigma_j - h\sum_{i\in\mathcal{C}} \sigma_i \, . \tag{11}$$

In a spin glass system, each J_{ij} is a random quantity [20]. Similarly to the RBMP, the set of values $\mathbf{J} = \{J_{ij}\}$ are i.i.d. random variables drawn from a particular probability distribution density $\rho(J)$. We extract $\mathbf{J}$ once for all pairs for each instance. This means that the disorder is **quenched** because these random variables do not vary with time – they are 'frozen'.

Remark 16: Sign of J_{ij}

The probability distribution $\rho(J)$ has to be such that it allows J_{ij} both to be negative or positive. Like this, we ensure that the model will exhibit both ferromagnetic and paramagnetic interactions.

Definition 9: The Edwards-Anderson (E-A) model

When $\mathcal{G}$ is a hypercubic lattice in d dimensions, the originated model is the Edwards-Anderson model. This is an example of disorder system, and more specifically, of a spin glass model.

Definition 10: The Sherrington-Kirkpatrick model (S-K) model

By considering a complete graph, i.e., $\mathcal{G} \equiv \mathcal{K}_{N,N}$, one arrives to the Sherrington-Kirkpatrick (S-K) model. This model is a mean-field version of the E-A model.

A generic **disordered system** is constituted by two main 'ingredients':

1. **Randomness**. In the E-A model, this is represented by the coupling constants J_{ij} being random variables.
2. **Frustration**. This phenomenon arises when there are local constraints conflictig with each other [20]. For example, in the 2-dimensional E-A model, when there is a cycle of four sites where three edges have $J_{ij} < 0$ and one of them, $J_{ij} < 0$. One can easily see that there is no configuration of Ising spins that can minimise all energy contributions of the edges independently. This gives rise to the fact that the energy landscape, and hence, the minimum energy configuration, has not a simple and predictable structure at all.

We are interested in averaging over the disorder. In the case of the E-A model, over all values of $\mathbf{J}$. From here on, we will represent the average of a function with respect to $\mathbf{J}$ as $\overline{\bullet}$. When performing this average over thermodynamical functionals we have to be careful as it is not a trivial task.

Remark 17:

The free energy $F_{\mathcal{G}}$ for a disordered system on an arbitrary graph $\mathcal{G} = (\mathcal{V}, \mathcal{E})$ is a **self-averaging** property [20]. This means that

$$\lim_{|\mathcal{V}|\to\infty} \frac{\overline{F_{\mathcal{G}}^2}}{\overline{F_{\mathcal{G}}}^2} = 1.$$

However, the partition function is not self-averaging.

In order to calculate $\overline{F_{\mathcal{G}}}$ in the E-A model, we need to calculate $\ln Z_{\mathcal{G}}$ since

$$\overline{F_{\mathcal{G}}(\beta, \mathbf{J})} \coloneqq -\frac{\overline{\ln Z_{\mathcal{G}}(\beta, \mathbf{J})}}{\beta} = -\frac{1}{\beta}\left(\prod_{(ij)} \int \rho(J_{ij})\, \mathrm{d}J_{ij}\right) \ln Z_{\mathcal{G}}(\beta, \mathbf{J}). \tag{12}$$

The **replica trick** relies on the following identity to facilitate the calculation above:

$$\ln Z = \lim_{n \to 0} \frac{Z^n - 1}{n}.$$

Hence, the calculation of $\overline{\ln Z_{\mathcal{G}}(\beta, \mathbf{J})}$ is reduced to calculating $\overline{Z^n_{\mathcal{G}}(\beta, \mathbf{J})}$, which turns out to be a much easier computation. In a way, it is as if we were averaging over n copies or *replicas* of the system.

Remark 18:

In Parisi's solution to the S-K model, the free energy of a spin glass in the thermodynamic limit has multivalley structure, i.e., many minima are separated by infinitely high barriers. Each valley corresponds to a state, and **ergodicity breaking** occurs [20]. This means that the average evolution of the system can no longer be predicted from the trajectory of a 'typical' point. Ergodicity breaking is closely related to **replica symmetry breaking** and **slow dynamics** in disordered systems where a mean-field approximation has been introduced in our calculations, like it happens in the S-K model.

Remark 19: The Edward-Anderson order parameter

The **Edward-Anderson order parameter** q_{EA} quantifies, in a way, the level of order/disorder. When $\beta \to 0$ and the spins are randomly oriented, $q_{EA} = 0$. However, for $\beta \to \infty$, $q_{EA} = \overline{\langle \sigma_i \rangle} > 0$ since $\langle \sigma_i \rangle \neq 0$ for each instance.

4.3 The cavity method and belief propagation

The cavity method [30] [31] is a statistical mechanics technique originally designed to solve a specific instance of a random optimisation problem in the context of spin glass models, and particularly, the Sherrington–Kirkpatrick model. However, it has been proven to be a powerful tool too when it comes to finding the solution of optimisation problems, such as k-satisfiability [32] and graph coloring [33]. In the next paragraphs, I will outline the theory of this method following the main layout in [28], [34] and [23].

Suppose that we have an Ising-type system chracterised by N spin-like variables where $\vec{\sigma} = (\sigma_1, \ldots, \sigma_N)$ with $\sigma_i \in \{-1, +1\}$ fixes a configuration of the system. Let us

also assume that the energy function or Hamiltonian [1] of the system is of the form

$$H(\vec{\sigma}) = \sum_{a=1}^{M} E_a(\vec{\sigma}_{\partial a}) + \sum_{i=1}^{N} W_i(\sigma_i) \; . \tag{13}$$

Let us break down the meaning of each of the components of Eq. 13. E_a is a function defined on the subset $\vec{\sigma}_{\partial a}$, while the functions W_i depend only on one variables σ_i.

In order to understand better Eq. 13, we will introduce a graphical representation of the problem called **factor graph**. The factor graph is a bipartite graph defined by

$$\mathcal{F}_H = \mathcal{G}(\mathcal{V}_\sigma, \mathcal{V}_E; \mathcal{E}), \quad |\mathcal{V}_\sigma| = N, \quad |\mathcal{V}_E| = M, \quad \mathcal{E} \subseteq \mathcal{V}_\sigma \times \mathcal{V}_E \; .$$

The factor graph represents a system of

- N "variable" vertices $\mathcal{V}_\sigma = \{i\}_i$ that we associate to the N variables $\vec{\sigma}$ so that $i \leftrightarrow \sigma_i$;
- M "function" vertices $\mathcal{V}_E = \{a\}_a$ that we associate to the M terms (or interactions) $\{E_a\}_a$ in the Hamiltonian;
- $(i, a) \in \mathcal{E}$ iff $\sigma_i \in \vec{\sigma}_{\partial a}$.

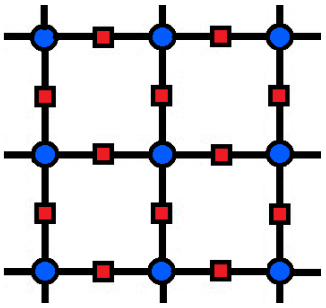

Figure 4: Factor graph of the Ising model on the 2-dimensional lattice with zero magnetic field. The red square nodes are the factor (or function) nodes, and the blue circle nodes are the variable nodes. Notice that there are no edges joining two nodes of the same color or type.

By applying the Cavity Method, one can in principle understand large systems like the one that is defined by the Hamiltonian in Eq. 13. The idea is to compare systems which only differ locally to the original one. These are called **cavity systems**. Cavity systems are devised in such a way that observables that are highly correlated and close to the deformation are almost uncorrelated, but minimally perturb other observables

[1] NB the change in notation here in order to avoid confusion between the Hamiltonian of the system H and E_a

that are far from the deformation (Cavity assumption) [34].

In fact, the cavity method has its foundations on local modifications of the factor graph, and on the study of the new system versus the old one, as mentioned above. This procedure is carried out in three 'steps'.

First, considering the system's Hamiltonian in Eq. 13, with $(i, a) \in \mathcal{E}$ being an edge on the factor graph, introduce a new modified Hamiltonian with $N + 1$ variables

$$H_{a \not\sim i}(\vec{\sigma}_{i_a}) = \sum_{b \neq a} E_b(\vec{\sigma}_{\partial b}) + E_a(\vec{\sigma}_{\partial a}^{\, i \longleftrightarrow i_a}) + \sum_{i=1}^{N} W_i(\sigma_i) \ , \tag{14}$$

where $\vec{\sigma}_{i_a} = \vec{\sigma} \cup \{\sigma_{i_a}\}$, and σ_{i_a} is the 'new' variable. $E_a(\vec{\sigma}_{\partial a}^{\, i \longleftrightarrow i_a})$ denotes that E_a is evaluated on all variables but the variable σ_i that has been substituted with the variable σ_{i_a}. Notice that, in the last term, the sum is run from $i = 1$ to $i = N$ rather than to $i = N + 1$. This is depicted in Figure 5, top right diagram, as removing an edge and inserting a new node.

In the same way that we defined Eq. 14, a function vertex can be removed, say a, which leads to a Hamiltonian with $M - 1$ function vertices (see Figure 5, bottom left diagram):

$$H_{\not a}(\vec{\sigma}) = \sum_{b \neq a} E_b(\vec{\sigma}_{\partial b}) + \sum_{i=1}^{N} W_i(\sigma_i) \ , \tag{15}$$

Another variation that we can apply to the factor graph is removing a variable vertex i and adding $|\partial i|$ variables σ_{i_b}, one for each b so that $\sigma_i \in \vec{\sigma}_{\partial b}$ (see Figure 5, bottom right diagram):

$$H_{\not i}(\vec{\sigma}_{\not i}) = \sum_{b:\, \sigma_i \notin \vec{\sigma}_{\partial b}} E_b(\vec{\sigma}_{\partial b}) + \sum_{b:\, \sigma_i \in \vec{\sigma}_{\partial b}} E_b(\vec{\sigma}_{\partial b}^{\, i \longleftrightarrow i_b}) + \sum_{j \neq i} W_j(\sigma_j) \ , \tag{16}$$

where we denoted $\vec{\sigma}_{\not i} \coloneqq (\vec{\sigma} \setminus \{\sigma_i\}) \cup \bigcup_{b:\, \sigma_i \in \vec{\sigma}_{\partial b}} \{\sigma_{i_b}\}$.

Hence, the Hamiltonian in Eq. 16 now has $N - 1 + |\partial i|$ spin variables, and once more one body contributions for the new variables were not introduced, i.e., no $W_i(\sigma_{i_b})$.

In Figure 5, it can be seen that introducing these new modified Hamiltonians create a local gap, hole or *cavity* in the factor graph, which is in a way a 'local perturbation' of the initial factor graph. In fact, having newly-defined Hamiltonians implies that their respective thermodynamical functionals can be obtained as well.

In analogy with the three modified Hamiltonians that we described above, three types of 'magnetic' fields can be defined on these graphs:

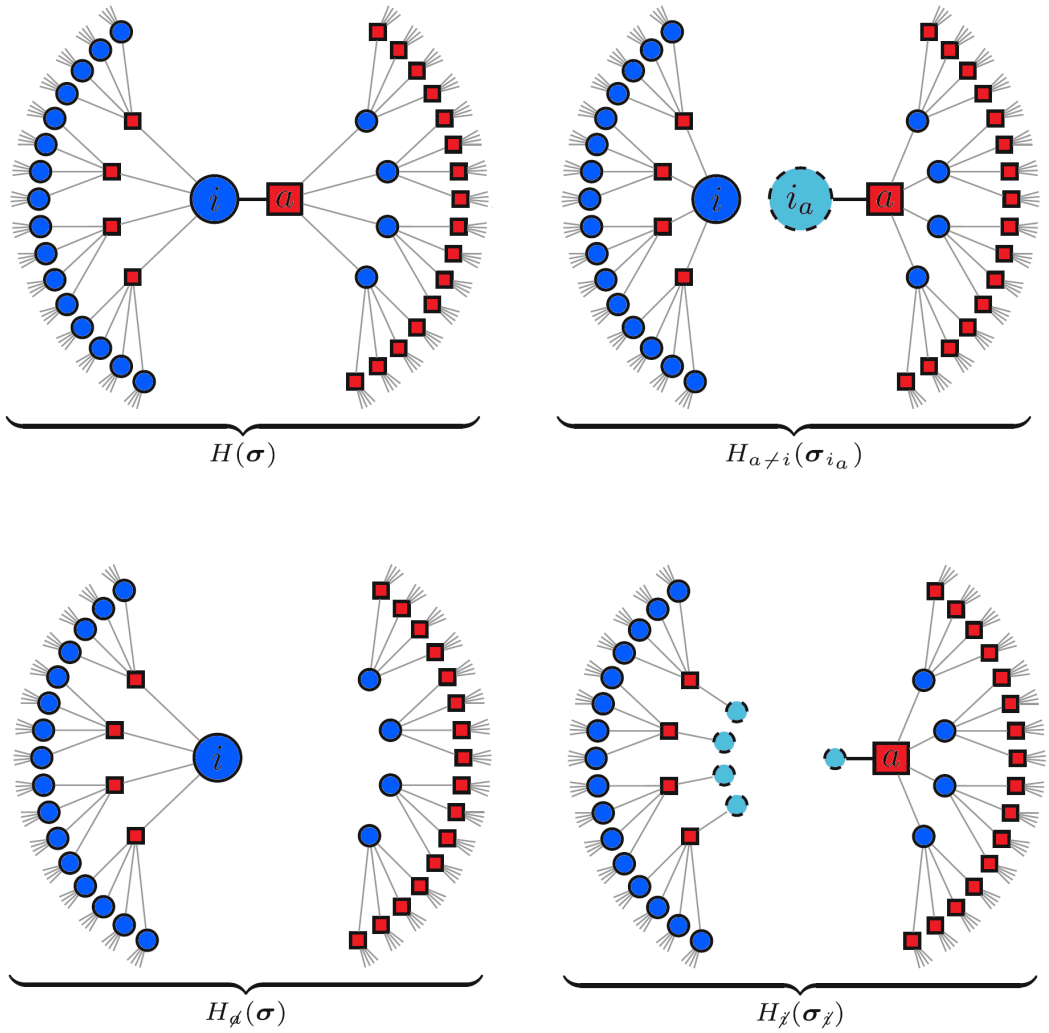

Figure 5: Diagrams adapted from [20]. Top left diagram shows the factor graph of the original Hamiltonian. The top right diagram represents the factor graph that originates when we add a new variable σ_{i_a}, i.e., when we remove the edge joining i to a and insert a new node i_a in light blue. The bottom left diagram shows the factor graph that we get after removing a function vertex, say a. Bottom right diagram adds the dashed light blue variables that represent σ_{i_b}. In order to see the differences between the original and the newly-defined Hamiltonians, compare every diagram with the top left one, the original one.

- The local **magnetic field** h_i acting on the spin σ_i. By considering the original Hamiltonian, the magnetic field interpretation of h_i arises from writing

$$P(\sigma_i = \sigma) \equiv \langle \delta_{\sigma_i\, \sigma} \rangle = \frac{e^{-\beta h_i \sigma}}{2\cosh(\beta h_i)} \,. \tag{17}$$

- The **cavity field** $h_{i\to a}$. Consider Eq. 16. Then, we define $h_{i\to a}$ to be such that

$$P(\sigma_i = \sigma) \equiv \langle \delta_{\sigma_i\, \sigma} \rangle_{i \not\to a} = \frac{e^{-\beta h_{i\to a} \sigma}}{2\cosh(\beta h_{i\to a})} \,. \tag{18}$$

- The **cavity bias** $u_{a\to i}$. For the same Hamiltonian as above, i.e., for the one in Eq. 16, we can also define $u_{a\to i}$ such that

$$P(\sigma_{i_a} = \sigma) \equiv \langle \delta_{\sigma_{i_a}\, \sigma} \rangle_{i \not\to a} = \frac{e^{-\beta u_{a\to i} \sigma}}{2\cosh(\beta u_{a\to i})} \,. \tag{19}$$

Now, let us introduce the **cavity ansatz**, which we will require to hold.

Definition 11: The cavity ansatz

In the $N \longrightarrow \infty$ limit, we assume that the follow approximations in a pure state

$$\Big\langle \prod_{b\in\partial i} \delta_{\sigma_{i_b}\sigma} \Big\rangle_{\not i} \simeq \langle \prod_{b\in\partial i} \delta_{\sigma_{i_b}\sigma} \rangle_{\not i} \,, \tag{20}$$

$$\Big\langle \prod_{j\in\partial a} \delta_{\sigma_j\sigma} \Big\rangle_{\not a} \simeq \langle \prod_{j\in\partial a} \delta_{\sigma_j\sigma} \rangle_{\not a} \,, \tag{21}$$

hold for any variable node i and any factor node a. Furthermore,

$$\langle \delta_{\sigma_{i_a}\sigma} \rangle_{\not a} \simeq \langle \delta_{\sigma_{i_a}\sigma} \rangle_{i \not\to a} \,, \tag{22}$$

$$\langle \delta_{\sigma_i\sigma} \rangle_{\not a} \simeq \langle \delta_{\sigma_i\sigma} \rangle_{i \not\to a} \,. \tag{23}$$

Remark 20:

The cavity ansatz, sometimes also called **replica symmetric assumption**, requires that in the modified factor graphs, i.e., in the ones where there is a cavity, the correlations between both 'sides' of the cavity are *almost* negligible. The cavity ansatz is **exact for tree-like factor graphs** or if there are very long cycles in the factor graph so that these correlations decay fast enough in such cycles.

Definition 12: The cavity equations

Combining the cavity ansatz equations with Eqs. 17, 18 and 19, we arrive to the **cavity equations**:

$$\frac{e^{-\beta h_{i\to a}\sigma}}{2\cosh(\beta h_{i\to a})} \propto e^{\beta W_i(\sigma_i)} \prod_{b\in\partial i,\, b\neq a} \frac{e^{-\beta u_{b\to i}\sigma}}{2\cosh(\beta u_{b\to i})} \tag{24}$$

$$\frac{e^{-\beta u_{a\to i}\sigma}}{2\cosh(\beta u_{a\to i})} \propto \sum_{\vec{\sigma}_{\partial a}} \delta_{\sigma_i\sigma}\, e^{\beta E_a(\vec{\sigma}_{\partial a})} \prod_{j\in\partial a,\, j\neq i} \frac{e^{-\beta h_{j\to a}\sigma_j}}{2\cosh(\beta H_{j\to a})} \tag{25}$$

For the case where $W_i(\sigma_i) \equiv w_i\sigma_i$, the cavity equations can be expressed in a simpler form:

$$h_{i\to a} = w_i + \sum_{b\in\partial i,\, b\neq a} u_{b\to i}\ , \tag{26}$$

$$u_{a\to i} = \frac{1}{2\beta}\ln\frac{\sum_{\vec{\sigma}_{\partial a},\,\sigma_i=-1}\exp\left[-\beta E_a(\vec{\sigma}_{\partial a}) - \beta\sum_{j\in\partial a,\, j\neq i} h_{j\to a}\right]}{\sum_{\vec{\sigma}_{\partial a},\,\sigma_i=+1}\exp\left[-\beta E_a(\vec{\sigma}_{\partial a}) - \beta\sum_{j\in\partial a,\, j\neq i} h_{j\to a}\right]}\ . \tag{27}$$

Now that we have the equations above, we can write the free energy F of the original system in terms of $F_{i\not\sim a}$, $F_{\not a}$ and $F_{\not i}$ in analogy to the modified Hamiltonians:

$$F \simeq F_{i\not\sim a} - \frac{1}{\beta}\sum_{\sigma\in\{-1,1\}} \frac{e^{\beta(h_{i\to a}+u_{a\to i})\sigma}}{4\cosh(\beta h_{i\to a})\cosh(\beta u_{a\to i})}\ ; \tag{28}$$

$$F \simeq F_{\not a} - \frac{1}{\beta}\ln\sum_{\vec{\sigma}_{\partial a}} e^{-\beta E_a(\vec{\sigma}_{\partial a})} \prod_{i\in\partial a} \frac{e^{-\beta h_{i\to a}\sigma_i}}{2\cosh(\beta u_{a\to i})}\ ; \tag{29}$$

$$F \simeq F_{\not i} - \frac{1}{\beta}\ln\sum_{\sigma\in\{-1,1\}} e^{-\beta W_i(\sigma)} \prod_{a\in\partial i} \frac{e^{-\beta u_{a\to i}\sigma}}{2\cosh(\beta u_{a\to i})}\ . \tag{30}$$

Once again, combining these equations with the cavity equations, we get that, for $a \in \partial i$,

$$P(\sigma_i = \sigma) \propto \exp\left(-\beta W(\sigma_i) - \beta\sigma\sum_{b\in\partial i} u_{b\to i}\right) = \exp\left[-\beta\sigma(u_{a\to i} + h_{i\to a})\right]\ . \tag{31}$$

So far, we have studied the cavity method applied to a spin system. Nevertheless, it is easy to see that the cavity method is actually a quite general technique.

Basing ourselves on the cavity method, we can construct a *message-passing* algorithm [23] for the solution of combinatorial optimisation problems that is often called

belief propagation.

In analogy to the cavity method, suppose we have a model with N variables $\vec{x} = \{x_i\}_{i=1,\dots,N}$, and assume they have a joint probability of the form

$$\mu(\vec{x}) = \frac{1}{Z} \prod_{a=1}^{M} f_a(\vec{x}_{\partial a}), \tag{32}$$

where $\vec{x}_{\partial a} \subseteq \vec{x}$, and Z is a normalisation constant.

This type of probability measure can be represented by a factor graph characterised by

$$\mathcal{F}_\mu = \mathcal{G}(\mathcal{V}_x, \mathcal{V}_f; \mathcal{E}), \quad |\mathcal{V}_x| = N, \quad |\mathcal{V}_f| = M, \quad \mathcal{E} \subseteq \mathcal{V}_x \times \mathcal{V}_f \ .$$

Similarly to the cavity method, we associate each function vertex $a \in \mathcal{V}_f$ to the function $f_a(\vec{x}_{\partial a})$, and each variable vertex $i \in \mathcal{V}_x$ to the variable x_i. Now, we define on each edge of this bipartite graph two functions, each accounting for each direction in which the edge can be traversed.

For an edge $e = (i, a)$, we define the **messages** $v_{i\to a}(x)$ and $\nu_{a\to i}(x)$, elements of the same space as probability distribution functions. They satisfy the following normalisation conditions:

$$\sum_{i\in\partial a} v_{i\to a}(x) = 1 \ \forall a \ \ , \sum_{a\in\partial i} \nu_{a\to i}(x) = 1 \ \forall i \ . \tag{33}$$

Just like we did when describing the cavity method, we can build some iterative 'message-passing' equations in which we update messages on an edge based on the incoming messages on the tail of the directed edge. These are completely analogous to the cavity equations, and are called **belief propagation equations**.

Definition 13: Belief propagation (BP) equations

The belief propagation equations are, after t steps,

$$v^{t+1}_{i\to a}(x) \simeq \prod_{b\in\partial i\setminus a} \nu^t_{b\to i}(x) \ , \tag{34}$$

$$\nu^{t+1}_{a\to i}(x) \simeq \sum_{\vec{x}_{\partial a},\, x_i\equiv x} f_a(\vec{x}_{\partial a}) \prod_{j\in\partial a,\, j\neq i} \nu^t_{j\to a}(x_j) \ . \tag{35}$$

After T iterations, we can write

$$v^T_i(x_i) \simeq \prod_{a\in\partial i} \nu^{T-1}_{a\to i}(x_i) \ . \tag{36}$$

Remark 21: Convergence and limiting distributions

When the factor graph is a tree, the BP equations converge regardless of the initial conditions after at most $T^* = diam(F_\mu)$.

If $v_i^*(x)$ and $\nu_i^*(x)$ are the limiting distributions, they are related to the marginal distrubition corresponding to the variable on the site i as follows:

$$v_i^*(x_i) \equiv \sum_{x_j \neq x_i} \mu(\vec{x})$$

4.4 Belief propagation for the assignment problem

Let us look now at the RBMP defined on the weighted complete bipartite graph $\mathcal{K}_{N,N} = \mathcal{G}(\mathcal{V},\mathcal{U};\mathcal{E})$. Then, the cost function is

$$\mathcal{C}[M] \coloneqq \frac{1}{N} \sum_{ij} m_{ij} w_{ij} \ , \tag{37}$$

where $M = (m_{ij})_{ij}$ is the matching matrix such that $m_{ij} = 1$ if the edge (v_i, u_j) is in the matching and 0 otherwise, and w_{ij} is the weight assigned to the edge (v_i, u_j).

For a given matrix M, we can write a joint probability

$$\mu(M) = \prod_{ij} \delta\left(\sum_{i=1}^{N} m_{ij},\ 1\right) \delta\left(\sum_{j=1}^{N} m_{ij},\ 1\right) \frac{e^{-\beta N^{-1} m_{ij} w_{ij}}}{Z} \tag{38}$$

for positive, real β.

The BP equations on the fixed point, provided that the cavity ansatz is still satisfied, are

$$v_{(ij)\to i}(m) \simeq \nu_{j\to(ij)}(m) e^{-\beta N^{-1} m w_{ij}} \ , \tag{39}$$

$$\nu_{i\to(ij)}(m) \simeq \sum_{\{m_{kj}\}_{k\neq i}} \delta\left(m + \sum_{k\neq i} m_{kj},\ \ 1\right) \prod_{k\neq i} \nu_{(kj)\to j}(m_{kj}) \tag{40}$$

In order to take the relevant optimisation limit, i.e., $\beta \longrightarrow \infty$, let us define for each oriented edge $\vec{e_{ij}} = \overrightarrow{(v_i, u_j)}$ of the *original* complete bipartite graph,

$$X(\overrightarrow{e_{ij}}) \coloneqq \frac{1}{\beta} \ln \frac{\nu_{i\to(ij)}(1)}{\nu_{i\to(ij)}(0)} \quad \text{and} \tag{41}$$

$$X(\overleftarrow{e_{ij}}) \coloneqq \frac{1}{\beta} \ln \frac{\nu_{j\to(ij)}(1)}{\nu_{j\to(ij)}(0)} \tag{42}$$

for the other orientation.

By applying this change of variable, we get the following modified BP equations at finite β:

$$X^{t+1}(\overrightarrow{e_{ij}}) = \frac{-1}{\beta} \ln \sum_{k \neq i} \exp\left[\frac{\beta w_{kj}}{N} + \beta X^t(\overleftarrow{e_{ij}})\right] , \tag{43}$$

$$X^{t+1}(\overleftarrow{e_{ij}}) = \frac{-1}{\beta} \ln \sum_{k \neq j} \exp\left[\frac{\beta w_{ik}}{N} + \beta X^t(\overrightarrow{e_{ij}})\right] . \tag{44}$$

Taking the limit $\beta \longrightarrow \infty$ of the equations above leads us to the **min-sum algorithm** for the assignment problem:

$$X^{t+1}(\overrightarrow{e_{ij}}) = \min_{k \neq i} \left[w_{kj} N^{-1} - X^t(\overleftarrow{e_{ij}})\right] , \tag{45}$$

$$X^{t+1}(\overleftarrow{e_{ij}}) = \min_{k \neq j} \left[w_{ik} N^{-1} - X^t(\overleftarrow{e_{ik}})\right] . \tag{46}$$

The criterion to select an edge for the perfect matching (i.e. the occupancy criterion) is

$$X(\overrightarrow{e_{ij}}) + X(\overleftarrow{e_{ij}}) \geq 0 . \tag{47}$$

5 Weighted dimer coverings on the Aztec diamond: the random bipartite matching problem

5.1 Setting up the problem

Let $\mathcal{A}_n$ be the bipartite Aztec diamond graph of order n defined as in Section 2.4, i.e., with n nodes in each of the four outter diagonals, and with $\mathcal{A}_n = (\mathcal{V}_{red} \cup \mathcal{V}_{blue}, \mathcal{E})$.

The aim of this project is to study the properties of the random bipartite matching problem in the thermodynamic limit at finite β defined on the weighted $\mathcal{A}_n$. The weights $\{w(e)\}_{e \in \mathcal{E}}$ are i.i.d. random variables, and on every instance of the problem, they are drawn from the probability distribution $\rho(w) = \theta(w)\, e^{-w}$.

Let us define the cost function to be

$$\mathcal{C}[M] \coloneqq \sum_{ij} m_{ij} w_{ij} , \tag{48}$$

where $M = (m_{ij})_{ij}$ is the occupancy matrix such that $m_{ij} = 1$ if the edge (v_i, u_j) is in the matching and 0 otherwise, and w_{ij} is the weight assigned to the edge (v_i, u_j). Notice that this definition only makes sense when we are looking at optimal solutions in

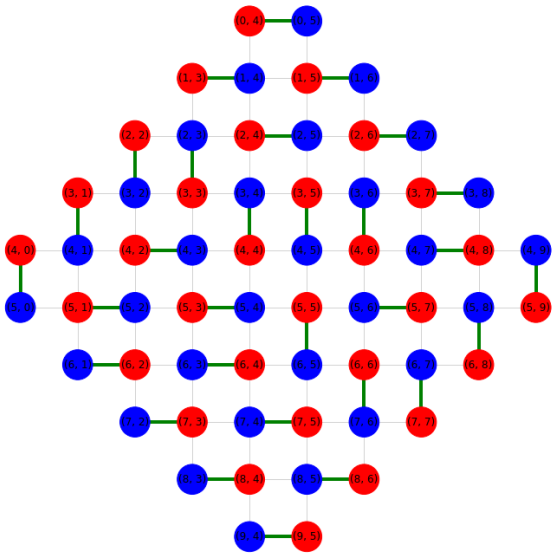

Figure 6: This figure represents one instance of the RBMP on the Aztec diamond graph of order $n = 5$ at $T = 0$. The edges in green are the ones that give the optimal cost in that configuration.

the limit of $T = 0$.

We are particularly interested on the average of the marginals of the edges of $\mathcal{A}_n$ over many realisations of the problem at finite β. The marginal of an edge is the probability that, when choosing a matching of $\mathcal{A}_n$ at random, the matching will include that specific edge. By studying these particular probability distributions, one can see if a frozen region emerges at finite T.

5.2 Methods

In order to find solutions and average properties of the RBMP that we are interested in, we used the message-passing algorithm of belief propagation. Notice that, since the Aztec diamond is not tree-like, we are using the loopy version of BP, a non-exact method, but a 'good enough' approximation for general graphs.

Pictorically, in order to implement BP, what we did was introducing a red field going from the red nodes to the blue nodes, and a blue field directed from blue nodes to red nodes. These, and their update rules, are represented by the slightly modified version of Eqns. 43 and 44:

$$X^{t+1}(\overrightarrow{e_{ij}}) = \frac{-1}{\beta} \ln \sum_{k \neq i} \exp\left[\beta w_{kj} + \beta X^t(\overleftarrow{e_{ij}})\right] ,$$
$$X^{t+1}(\overleftarrow{e_{ij}}) = \frac{-1}{\beta} \ln \sum_{k \neq j} \exp\left[\beta w_{ik} + \beta X^t(\overrightarrow{e_{ij}})\right] .$$

Notice that in the factor graph of the $\mathcal{A}_n$, the nodes are the factors, and the edges are the variables. Then, the outline of the loopy BP algorithm is as follows:

1. Initialise the fields/messages arbitrarily.
2. Sweep all nodes/factors in random order.
3. Use incoming fields/messages on a factor/node to update the outgoing ones.
4. Iterate this method until convergence.

Convergence of the messages is not ensured for $T > 0$. Therefore, in order to monitor convergence, we introduce the Bethe free energy [23]. It is calculated for every update of BP until it converges:

$$F(\beta) = \frac{-1}{\beta|\mathcal{V}|} \left[\sum_{v \in \mathcal{V}} \ln \sum_{e \in \partial v} e^{-\beta(w(e) - X(\overrightarrow{e_{ij}}))} - \sum_{e \in \mathcal{E}} \ln \left(1 + e^{-\beta(w(e) - X(\overrightarrow{e_{ij}}) - X(\overleftarrow{e_{ij}}))}\right) \right] .$$

Notice that $F(\beta \to \infty) = C(M)$. The BP equations are stationary points of the Bethe free entropy, i.e. $-\beta F(\beta)$.

As a 'sanity check', we calculated the average optimal cost of the complete bipartite graph with weight distribution $\rho(w) = \theta(w)\, e^{-w}$ and made sure the value was the same given by Parisi's theoretical formula.

The algorithm was constructed on Python from scratch, and in order to construct the graphs on Python, we used a module called NetworkX designed for graphical models.

5.3 Results

5.3.1 Bethe free energies

First, let us start by performing a consistency test. In Figure 7, we can see how the average Bethe free energy grows as we increase the temperature for all the orders n, which agrees with the physical interpretation – as we heat the system, there is more free energy available for the system to use.

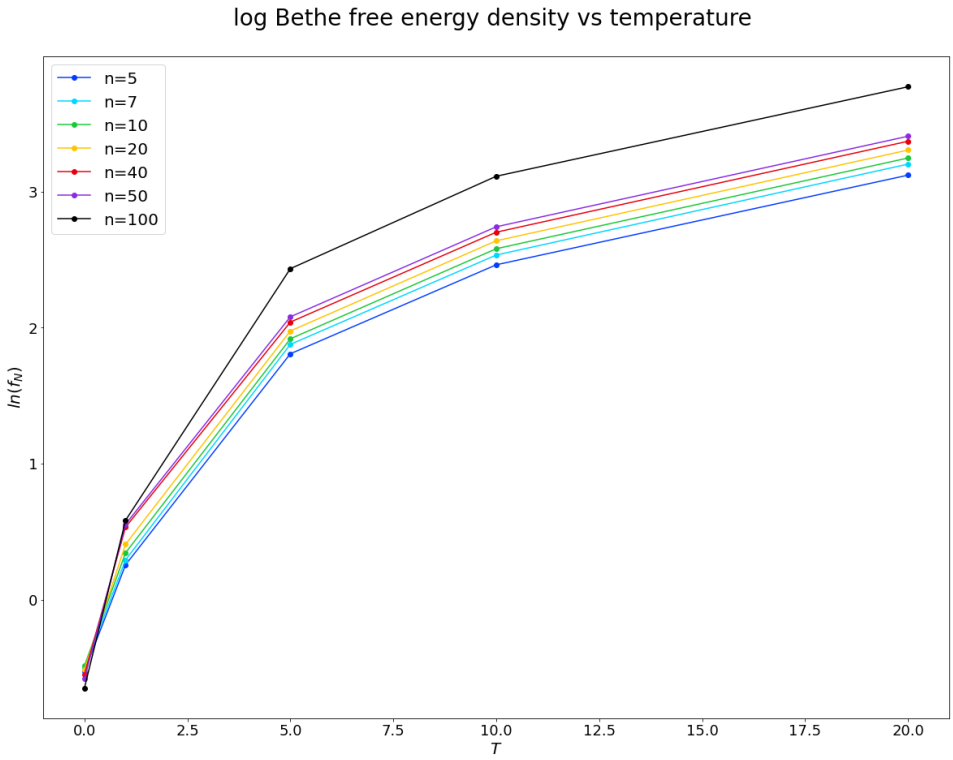

Figure 7: Plot of the log of the average Bethe free energies for Aztec diamonds of different orders vs temperature. The number of realisations was 100, except for $n = 50$ and $n = 100$, where the number of realisations was 10 due to time constraints.

This consistency check, however, does not ensure the accuracy of the marginals. It just ensures that the BP algorithm is indeed converging to some value(s).

5.3.2 Fixed n, varying T

In the Aztec diamond of order n, the Arctic Circle phenomenon emerges for $T \geq 5$ (see Figure 8). However, when we plot the heatmap of the marginals for order $n = 100$, as we increase the temperature (see Figure 9), it seems that the Arctic circle is starting to form as a liquid phase in the shape of a square with round corners starts to arise.

It seems that the higher the order of the Aztec diamond, the greater the temperature needed for the marginals to converge to the limit shape of the arctic circle. Another possibility would be that, because of the possible inaccuracy of BP in general graphs, the algorithm breaks down for large n and gives the incorrect marginals.

A counter argument for the latter is that Figure 10 and 11 seem consistent with each other in terms of limiting shapes.

As a curiosity, the heatmaps of the variance of the marginals for the Aztec diamond of order $n = 10$ (see Figure 12) and $n = 20$ show a limiting shape in the interior region that resembles a cross – an Aztec diamond inside an Aztec diamond.

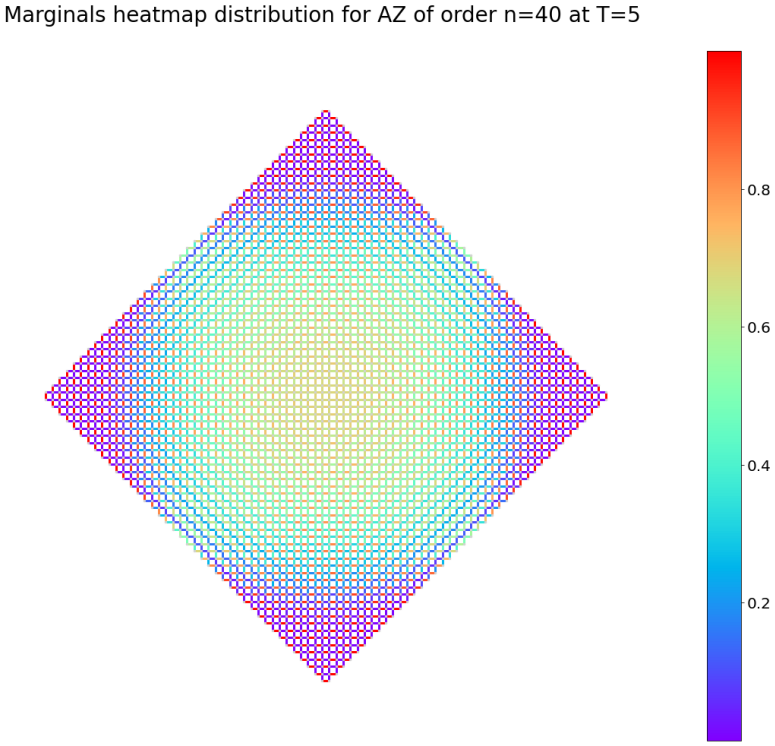

Figure 8: Heatmap of the average marginals distribution of the Aztec diamond of order 40 (100 realisations) at $T = 5$. The diamond exhibits a frozen region around its edges and and an inner liquid region in the shape of an inscribed circle. This is why in the outter area the edges are either in red (very likely to be occupied) or in purple (very unlikely to be occupied), and within the circle, the marginals attain more 'neutral' values.

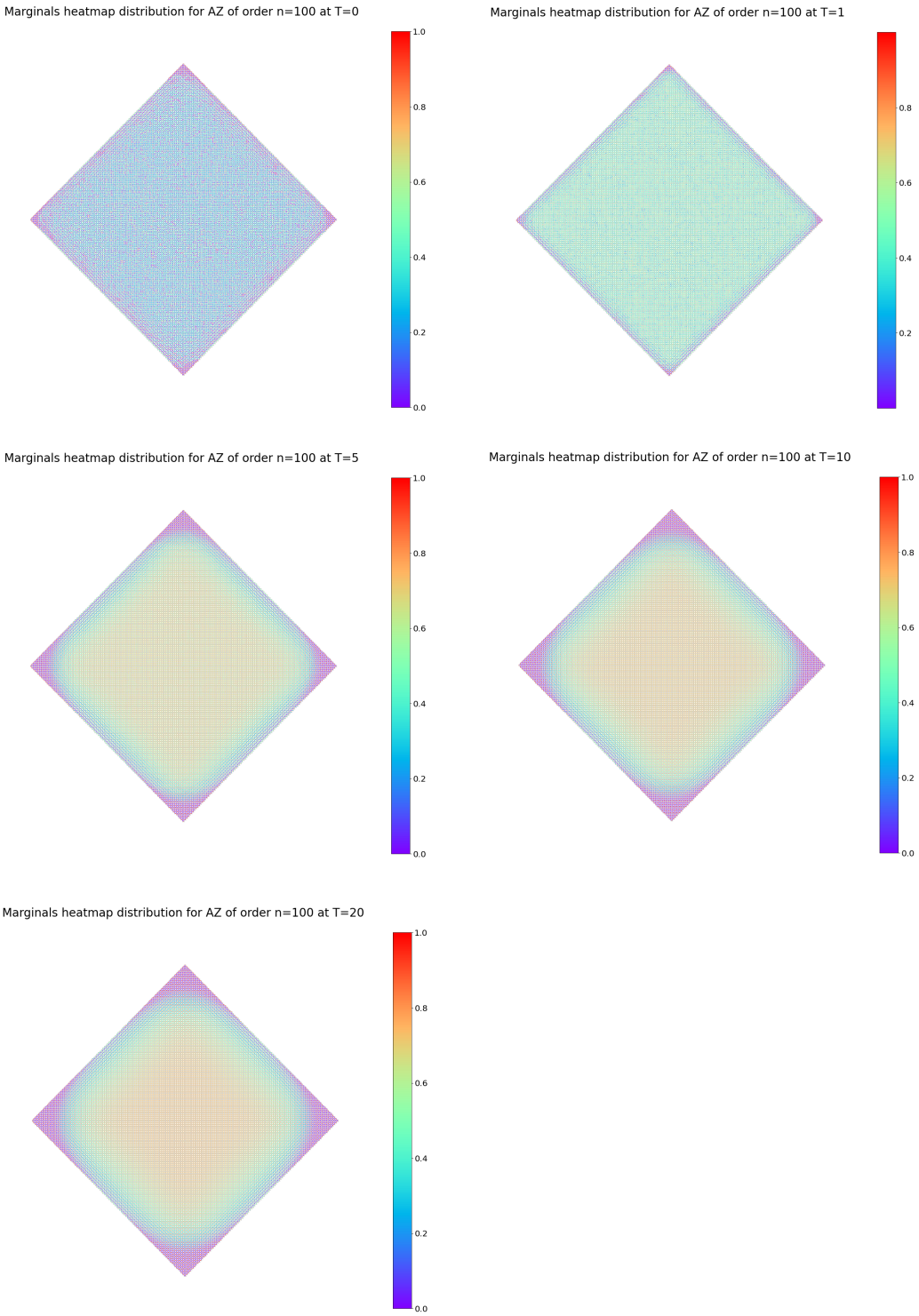

Figure 9: Heatmap of the average marginals distribution of the Aztec diamond of order 100 (10 realisations) at $T = 0, 1, 5, 10, 20$. The diamond starts to transition to an arctic circle regime, but it seems that the temperatures are not high enough for the circle to fully form.

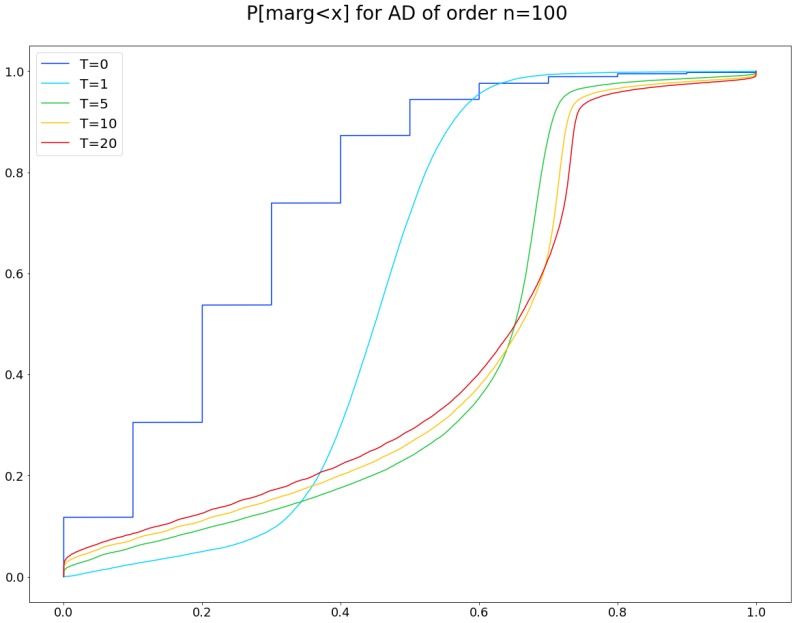

Figure 10: Probability that the marginal is less than x at different temperatures for the Aztec diamond of order $n = 100$.

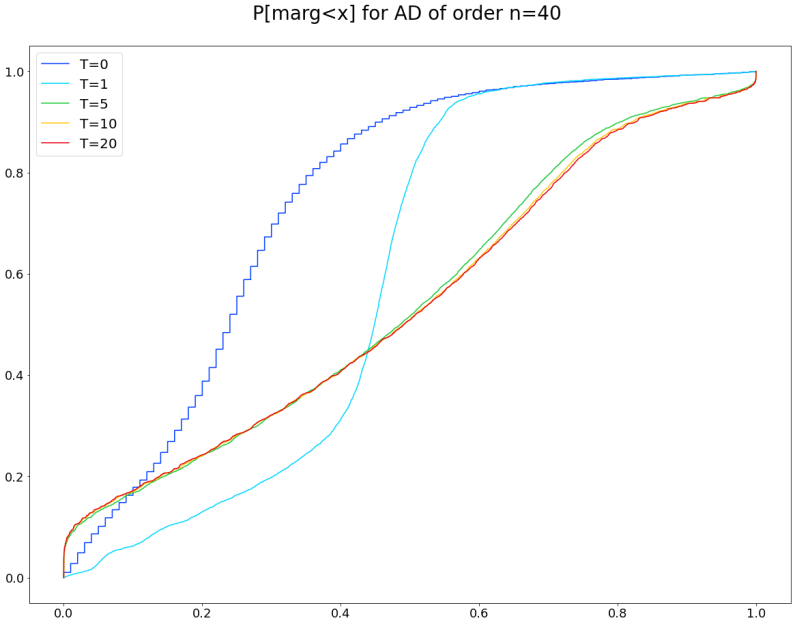

Figure 11: Probability that the marginal is less than x at different temperatures for the Aztec diamond of order $n = 40$.

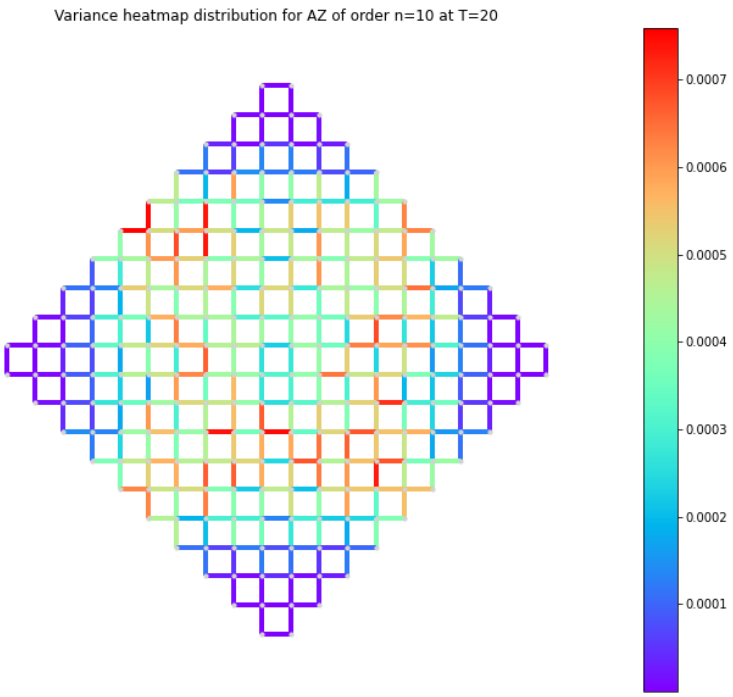

Figure 12: Heatmap of the variance of the marginals of the AD of order $n = 10$ (100 iterations).

5.3.3 Fixed T, varying n

Finally, we would like to address Figure 13. It is worth noting that, even though for $n = 50$ and $n = 100$ only 10 realisations of the problem were made, the curve look well-behaved, probably because of the self-averaging property as we increase n.

In Figure 13, it seems that the accumulative probability of the marginals tend to the classical limit for all n as we increase n except for $n = 100$. This might be because of what was mentioned before. A possibility is that, for $n \longrightarrow \infty$, we need to look at the curves for higher T in order to get a clearer discontinuity that confirms the emergence of a frozen region.

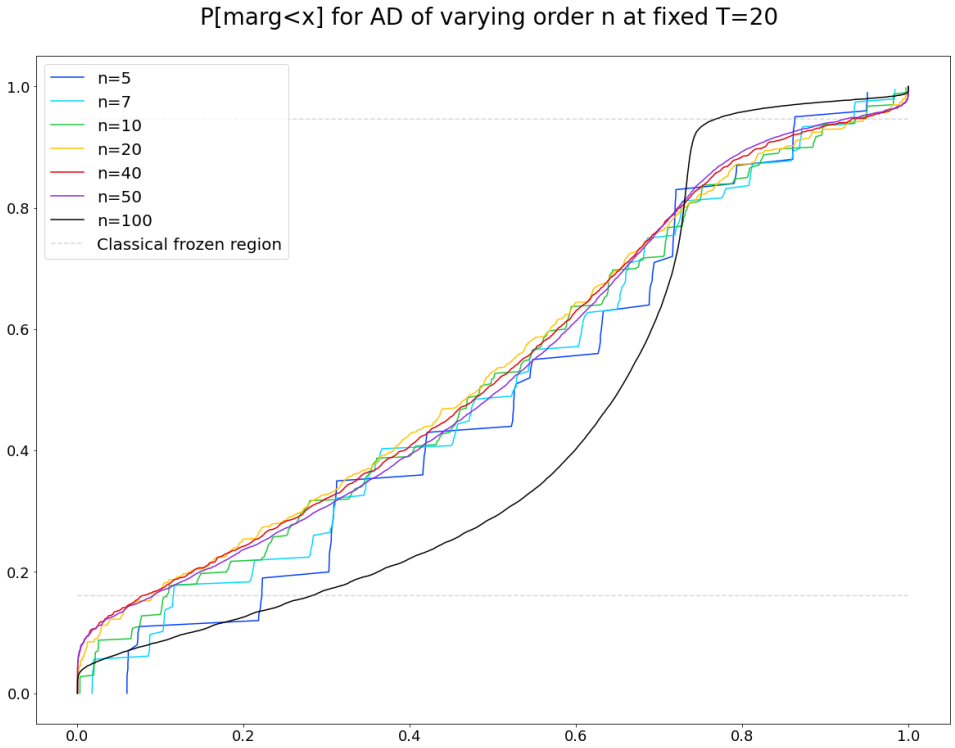

Figure 13: Plot of the probability that the marginals are less than x for different n, fixed $T = 20$.

5.4 Discussion and conclusions

One key improvement of the project that could not be done due to time constraints is checking how precise the marginals of the Aztec diamond in the results were. Loopy Belief Propagation does not guarantee that the marginals in graphical models that are not tree-like are exact. Therefore, one of the fitting next steps would be to check that the

marginals given after running BP on the Aztec diamond graph are indeed exact. This can be done by implementing the so-called **Generalised Domino-shuffling** algorithm [11]. This is a remarkable result as it is capable of:

- Finding the cost of the matchings of a weighted Aztec diamond graph A_n;
- Computing the marginal of a particular edge being included in a randomly-chosen matching of A_n;
- Randomly generating a perfect matching of A_n.

More computational power would have allowed us to perform a more exhaustive analysis of the random dimer covering problem on the Aztec diamond in the thermodynamic limit. For instance, the Aztec diamond of order 40 still showed prevalence of finite size corrections in its Bethe free energy, and nonetheless, it took several hours to run enough instances of the optimisation problem.

Another matter that could have been more exhaustively studied (given more powerful computational resources) is under which definite conditions the arctic circle appears on the weighted Aztec diamond. Some open questions about this include:

- Is there a critical temperature for which the arctic circle arises?
- Is this critical temperature dependant on the size of the Aztec diamond?
- How does changing the probability distribution affect the appearance of the arctic circle?

Further work on the weighted Aztec diamond could consist of studying excitations of the model by cutting an edge and seeing how this affects the matchings depending on the region where the edge is positioned. Criticality and comformality of the model is definitely another direction that could be considered as next focus.

In conclusion, the random dimer covering problem on the Aztec diamond is a research topic that still has a lot to offer given some of the counterintuitive and non-expected results that we obtained. Creating a united front with mathematicians, physicists and computer scientists would definitely contribute towards creating a 'theory of everything' of combinatorial optimisation, statistical mechanics and algorithms for graphical models and assignment with faster and more powerful tools.

References

[1] H. Sachs and H. Zernitz, "Remark on the dimer problem," *Discrete Applied Mathematics*, vol. 51, no. 1-2, pp. 171–179, 1994.

[2] F. Ardila and R. P. Stanley, "Tilings," *The Mathematical Intelligencer*, vol. 32, no. 4, pp. 32–43, 2010.

[3] W. P. Thurston, "Conway's tiling groups," *The American Mathematical Monthly*, vol. 97, no. 8, pp. 757–773, 1990.

[4] P. Hall, "On representatives of subsets," in *Classic Papers in Combinatorics*, pp. 58–62, Springer, 2009.

[5] P. W. Kasteleyn, "The statistics of dimers on a lattice: I. the number of dimer arrangements on a quadratic lattice," *Physica*, vol. 27, no. 12, pp. 1209–1225, 1961.

[6] H. N. Temperley and M. E. Fisher, "Dimer problem in statistical mechanics-an exact result," *Philosophical Magazine*, vol. 6, no. 68, pp. 1061–1063, 1961.

[7] M. E. Fisher, "Statistical mechanics of dimers on a plane lattice," *Physical Review*, vol. 124, no. 6, p. 1664, 1961.

[8] E. H. Lieb, "Solution of the dimer problem by the transfer matrix method," *Journal of Mathematical Physics*, vol. 8, no. 12, pp. 2339–2341, 1967.

[9] G. Benkart and O. Eng, "Weighted aztec diamond graphs and the weyl character formula," *the electronic journal of combinatorics*, pp. R28–R28, 2004.

[10] W. Jockusch, J. Propp, and P. Shor, "Random domino tilings and the arctic circle theorem," *arXiv preprint math/9801068*, 1998.

[11] J. Propp, "Generalized domino-shuffling," *Theoretical Computer Science*, vol. 303, no. 2-3, pp. 267–301, 2003.

[12] É. Janvresse, T. De La Rue, and Y. Velenik, "A note on domino shuffling," *Electronic Journal of Combinatorics*, vol. 13, no. 1, p. R30, 2006.

[13] E. Noam, K. Greg, L. Michael, and P. James, "Alternating sign matrices and domino tilings," 1991.

[14] J. J. Rué Perna, "Domino tilings of the aztec diamond," *Snapshots for modern mathematics from Oberwolfach*, no. 16, pp. 1–11, 2015.

[15] W. H. Mills, D. P. Robbins, and H. Rumsey Jr, "Alternating sign matrices and descending plane partitions," *Journal of Combinatorial Theory, Series A*, vol. 34, no. 3, pp. 340–359, 1983.

[16] D. Zeilberger, "Proof of the alternating sign matrix conjecture," *arXiv preprint math/9407211*, 1994.

[17] G. Kuperberg, "Another proof of the alternative-sign matrix conjecture," *International Mathematics Research Notices*, vol. 1996, no. 3, pp. 139–150, 1996.

[18] R. Kenyon, "An introduction to the dimer model," *arXiv preprint math/0310326*, 2003.

[19] S. Sheffield, "Gaussian free fields for mathematicians," *Probability theory and related fields*, vol. 139, no. 3-4, pp. 521–541, 2007.

[20] G. Sicuro, "Euclidean matching problems," in *The Euclidean Matching Problem*, pp. 59–118, Springer, 2017.

[21] H. W. Kuhn, "The hungarian method for the assignment problem," *Naval research logistics quarterly*, vol. 2, no. 1-2, pp. 83–97, 1955.

[22] G. B. Dantzig and M. N. Thapa, *Linear programming 1: introduction*. Springer Science & Business Media, 2006.

[23] M. Mezard and A. Montanari, *Information, physics, and computation*. Oxford University Press, 2009.

[24] K. Huang, *Introduction to statistical physics*. Chapman and Hall/CRC, 2009.

[25] D. J. Aldous, "The ζ (2) limit in the random assignment problem," *Random Structures & Algorithms*, vol. 18, no. 4, pp. 381–418, 2001.

[26] M. Mézard and G. Parisi, "Replicas and optimization," *Journal de Physique Lettres*, vol. 46, no. 17, pp. 771–778, 1985.

[27] G. Parisi, "A conjecture on random bipartite matching," *arXiv preprint cond-mat/9801176*, 1998.

[28] A. Annibale, "Dynamical analysis of complex systems lecture notes," 2020-21.

[29] H. Nishimori, *Statistical physics of spin glasses and information processing: an introduction*. No. 111, Clarendon Press, 2001.

[30] M. Mézard and G. Parisi, "The bethe lattice spin glass revisited," *The European Physical Journal B-Condensed Matter and Complex Systems*, vol. 20, no. 2, pp. 217–233, 2001.

[31] M. Mézard and G. Parisi, "The cavity method at zero temperature," *Journal of Statistical Physics*, vol. 111, no. 1, pp. 1–34, 2003.

[32] M. Mézard and R. Zecchina, "Random k-satisfiability problem: From an analytic solution to an efficient algorithm," *Physical Review E*, vol. 66, no. 5, p. 056126, 2002.

[33] T. Castellani, V. Napolano, F. Ricci-Tersenghi, and R. Zecchina, "Bicolouring random hypergraphs," *Journal of Physics A: Mathematical and General*, vol. 36, no. 43, p. 11037, 2003.

[34] C. Grosso, "Cavity method analysis for random assignment problems," *Universita degli Studi di Milano (2002-2003)*, 2004.